Electronic Supplementary Material (ESI) for Journal of Materials Chemistry C.

Electronic Supplementary Informations

The disentangling of hysteretic spin transition, polymorphism and metastability in bistable thin films formed by sublimation of bis(scorpionate) Fe(II) molecules

O. Iasco,[a] M.-L. Boillot[a*], A. Bellec,[b] T. Mallah,[a] R. Guillot,[a] E. Rivière,[a] S. Mazerat,[a]
S. Nowak,[c] V. Repain,[b] D. Morineau,[d] A. Brosseau[e] and F. Miserque,[f] V. Repain[b] and T. Mallah[a*]

Content

Table ST1: Crystal data and structure refinement for the triclinic (at 100, 240 and 298 K) and tetragonal (at 253 K) polymorphs of Fe[HB(3,5-$(Me)_2Pz)_3]_2$.

	$Fe[HB(3,5\text{-}(Me)_2Pz)_3]_2$			
Empirical formula	$C_{30}\ H_{44}\ B_2\ Fe\ N_{12}$			$C_{30}\ H_{44}\ B_2\ Fe\ N_{12}$ [a]
Formula weight	650.24			
Temperature (K)	100(1)	240(1)	298(1)	253(1)
Color	pink	colorless	colorless	colorless
Wavelength (Å)	0.71073			
Crystal system	triclinic			tetragonal
Space group	*P* -1			*P -4 2₁ m*
a (Å)	8.7244(5)	8.7770(9)	8.8124(3)	20.669(5)
b (Å)	10.4918(6)	10.7908(10)	10.1928(3)	20.669(5)
c (Å)	10.8211(6)	10.9916(17)	10.7673(4)	8.603(3)
α (°)	115.322(2)	106.485(7)	116.3380(10)	90
β(°)	98.499(3)	108.711(7)	85.244(2)	90
γ(°)	109.477(3)	109.714(5)	100.143(2)	90
V ($Å^3$)	793.58(8)	833.7(2)	853.19(5)	3675(2)
Z ; Z'	1 ; 0,5			4 ; 1
Density (calc.) ($g.cm^{-3}$)	1.361	1.295	1.266	1.175 [a]
Abs. coefficient (mm^{-1})	0.518	0.493	0.482	0.411
F(000)	344			1376 [a]
Crystal size (mm)	0.06 x 0.02 x0.009		0.110 x 0.03 x 0.010	0.03 x 0.02 x 0.01
θ range (°)	2.215 - 30.647	2.232 - 30.549	2.257 - 30.564	2.203 - 20.694
h	-12 – 12	-12 – 12	-12 – 12	-20 – 20
k	-15 – 15	-15 – 15	-14 – 14	-20 – 20

l	-15 – 15	-15 – 15	-15 – 15	-8 – 8
No. of reflections collected	26 912	29 746	50 969	42 038
No. of independent reflections	4 888	5 099	5 236	1 998
R_{int}	0.0660	0.0742	0.0401	0.3063
Data/restraints/parameters	3749 / 0 / 211	3460 / 0 / 211	3766 / 0 / 211	712 / 24 /117
Goodness-of-fit on F^2	1.119	1.094	1.082	1.035
$R1$ [$I > 2\sigma(I)$]	0.0554	0.0636	0.0488	0.1233
$wR2$ [$I > 2\sigma(I)$]	0.1243	0.1429	0.0879	0.2503
$R1$ (all data)	0.0862	0.1140	0.1275	0.3011
$wR2$ (all data)	0.1413	0.1656	0.1523	0.3314
Largest diff. hole and peak (e-.Å^{-3})	-0.812 ; 0.574	-0.512 ; 0.459	-0.551 ; 0.511	-0.487 ; 1.035

Number of crystallographic independent molecules Z' = Z / number of symmetry operations (in the Table of space group) [a] The formula does not include the solvent that is disordered.

Table ST2 : Structural parameters characterizing the Fe[HB(3,5-$(Me)_2Pz)_3]_2$ molecule in the triclinic polymorph.

Temperature (K)	Spin-state	Fe-N (Å)	Fe…B (Å)	<Fe-N> (Å) (a□	Σ (°), θ (°) □a□	Fe-N_2-N_1-C_5 (°)	Fe-N_2-N_1-B (°)
100	LS	1.991(2)	3.065	1.995	2.4, 5	178.5	1.4
		1.997(2)					
		1.997(2)					
240	~80% HS	2.136(2)	3.164	2.140	35.5, 46	176.4	2.6
		2.141(2)					
		2.144(2)					
298	HS	2.160(2)	3.182	2.178	39.9, 54	174.2	6.5
		2.185(2)					
		2.189(2)					

$$\Sigma = \sum_{i=1}^{12} |90 - \alpha i| \quad \theta = \sum_{j=1}^{24} |60 - \theta j|$$

(a) <Fe-N>, average Fe-N bond length, □

Preparation of the as-sublimed films of $Fe^{II}[HB(3,5\text{-}(Me)_2Pz)_3]_2$. The deposition on surfaces was done either in a chamber under secondary vacuum (ca. 10^{-5} mbar, T_S=125 °C, series 1) or in a chamber under ultra-high vacuum (ca. 5.10^{-8} mbar, T_S in the range of 120°C to 140°C, series 2). In the first case (series 1), the substrate (quartz, silicon wafer or gold) was placed at 210 mm above the evaporation source. After the pressure stabilization, the crucible was heated at 4°C/min up to 125 °C then, the temperature was kept constant once the nominal deposition rate reaches the value of 1 Å s^{-1}. This rate, as well as the nominal thickness of deposited matter (fixed here at 190 nm), was evaluated with a quartz crystal microbalance. Then the effective thickness of the film was determined using a KLA- Tencor D-120 Profilometer: 130 ± 13 nm. The samples of series 2 were obtained by the sublimation from a home-made evaporator (Knusden cell type) in a UHV chamber with a base pressure of 5.10^{-8} mbar. Thanks to a mask, the set-up enables the fabrication of four samples at the same time and the sublimation procedure has been repeated. Each time the sublimation temperature has been stabilized between 120 and 140°C. During the sublimation, the evaporator crucible is at a distance of ca. 60 mm from the quartz samples. The sample thicknesses were measured afterwards using a Dektak-150 (Brucker) profilometer. All the samples presented the same characteristics especially concerning the structural properties.

Table **ST3** : Thickness, roughness, RMS data determined for the layers of $Fe[HB(3,5\text{-}(Me)_2Pz)_3]_2$

Thickness (nm)	90 (40)	130 (13) (ζ)	160 (10)	1740 (110)	2660 (90)	3470 (60)	8020 (150) (κ)	8460 (230)
Roughness (nm)	9(4)	-	7(3)	18(10)	21(7)	30(13)	176(64)	75(19)
RMS (nm)	-	20	-	-	-	-	>90	-

Roughness and RMS values determined using a profilometer and AFM respectively. ζ and κ labels correspond to the films denoted **1** and **2** respectively.

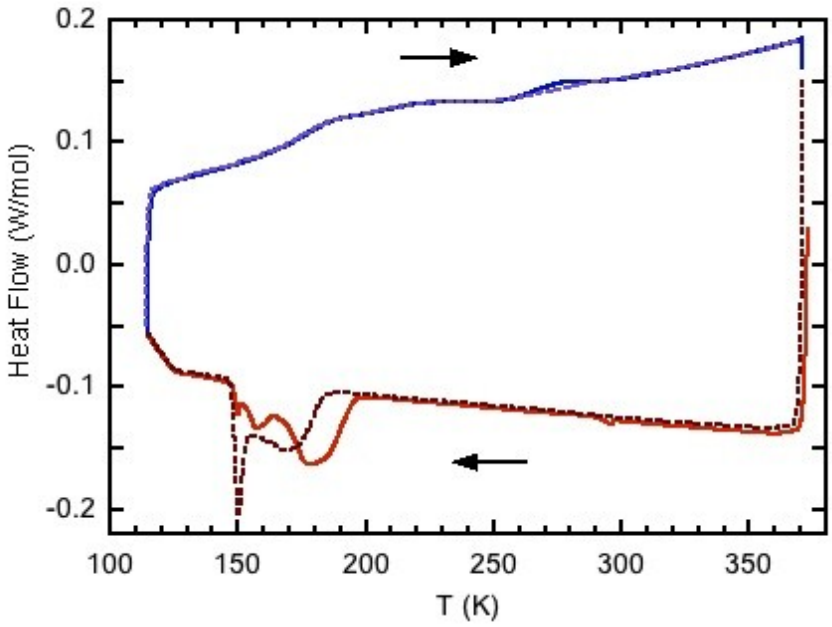

Fig. S1: DSC analysis of the as-synthesized sample of $Fe[HB(3,5\text{-}(Me)_2Pz)_3]_2$. Overlay of the first thermal cycle (—) and the second one (---) collected between 373 and 113 K at 10 $Kmin^{-1}$.

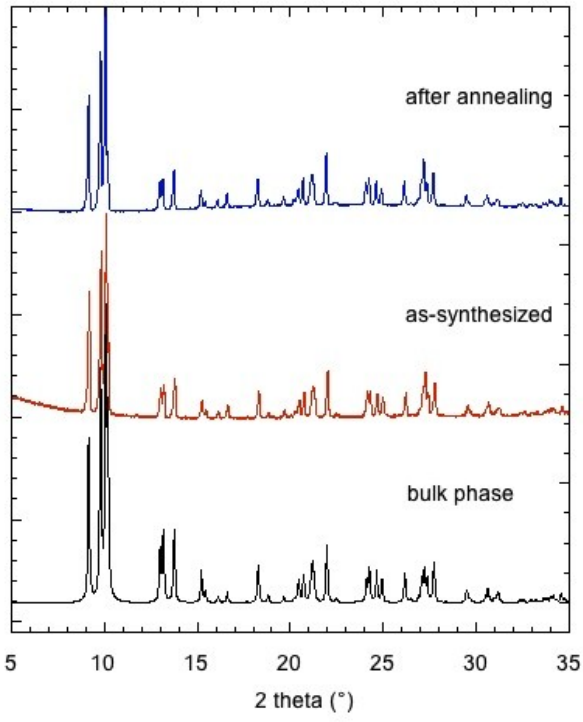

Fig. S2: Superimposition of X-ray diffractograms of the as-synthesized polycrystalline powder at RT before and after the annealing at 100°C, and that calculated from the 298 K single-crystal structure.

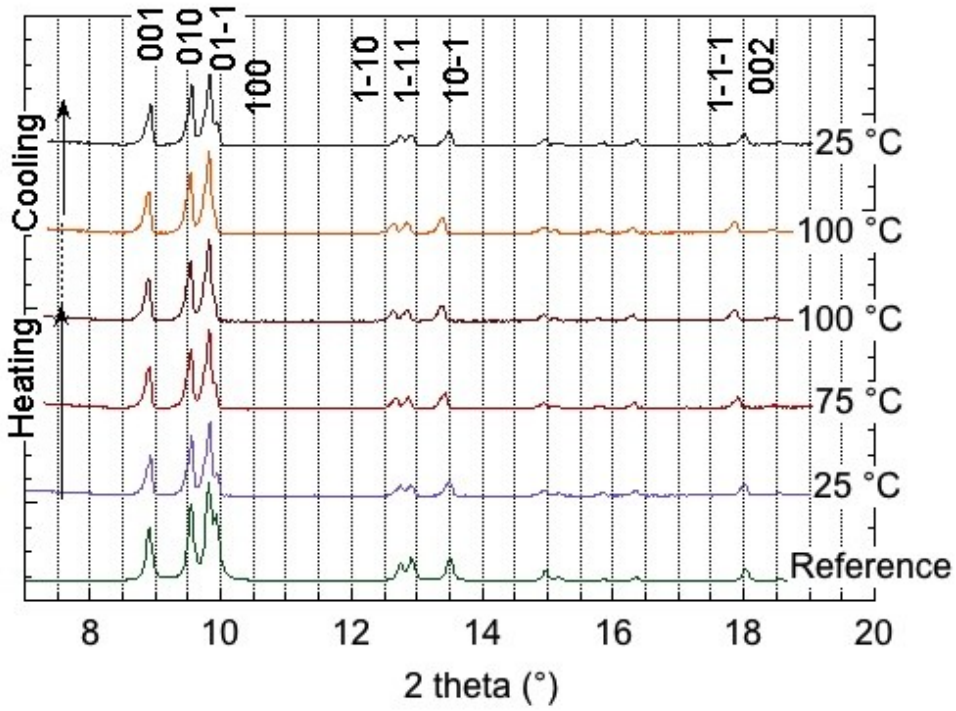

(a)

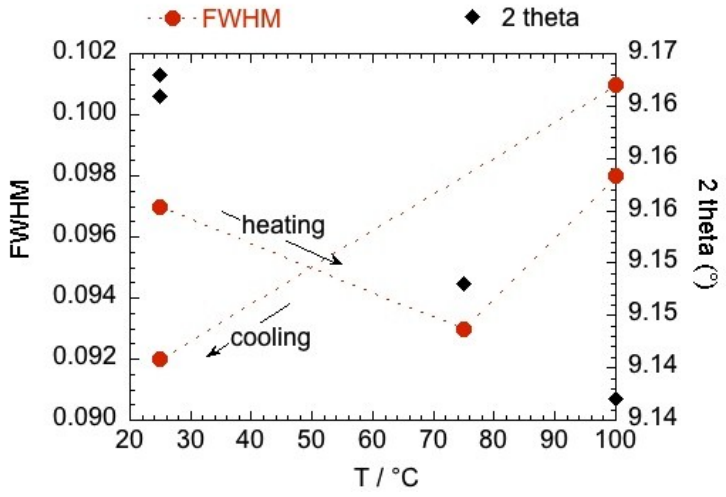

(b)

Fig. S3 : (a) Thermal evolution of the X-ray diffractograms of the as-synthesized powder between 25 and 100 °C then again at 25 °C; (b) Temperature dependence of the values of the full width at half maximum (FWHM) and the 2 theta angle for the (001) Bragg peak.

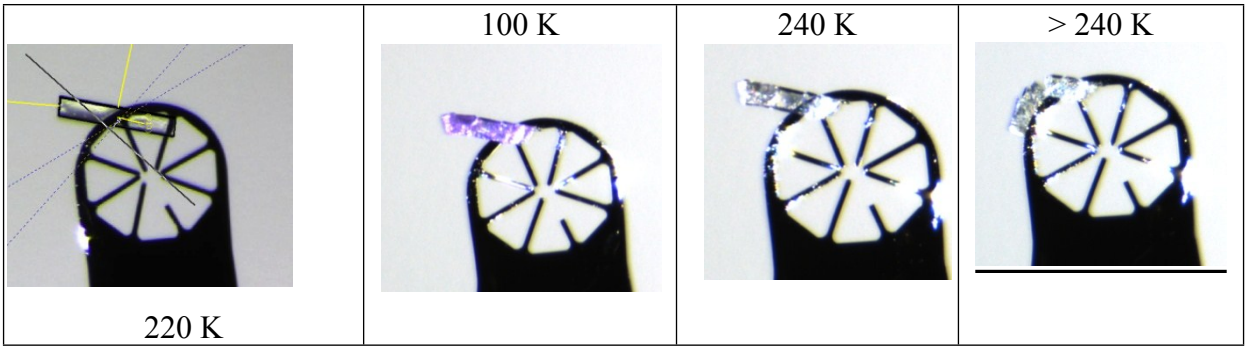

Fig. S4 : Photographs of the single-crystal successively maintained at 220, 100 and 240 K for the collection of X-ray diffraction data, then of the crystal shattering above 240 K.

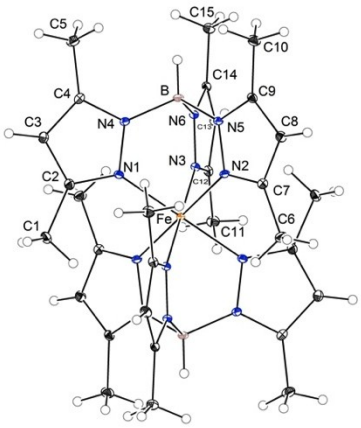

Fig.S5: An ORTEP view of $Fe[HB(3,5\text{-}(Me)_2Pz)_3]_2$ at 100 K with displacement ellipsoids drawn at the 30% probability level. H atoms are represented as small spheres of arbitrary radii.

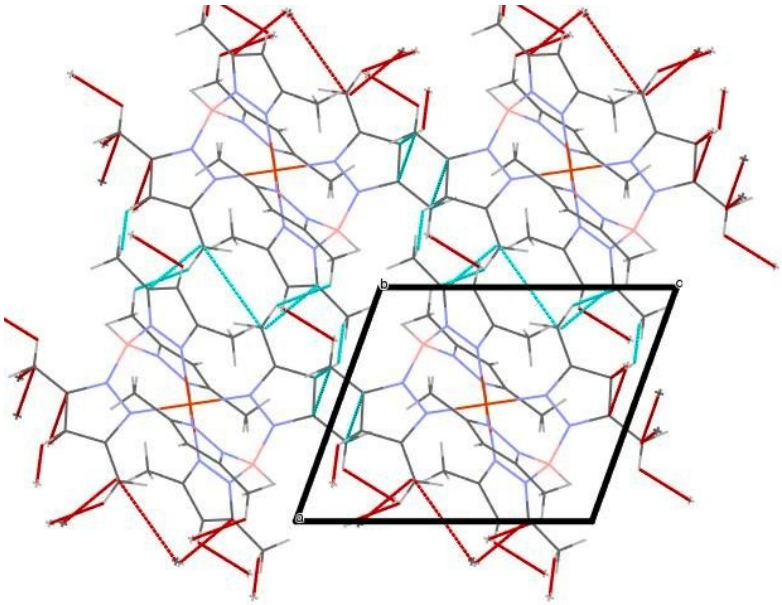

Fig. S6: View of the molecular packing of $Fe[HB(3,5\text{-}(Me)_2Pz)_3]_2$ (T = 100 K) within the *(010)* plane with the Van der Waals interactions involving Me, C (HC) groups of two (three) pyrazolyl rings.

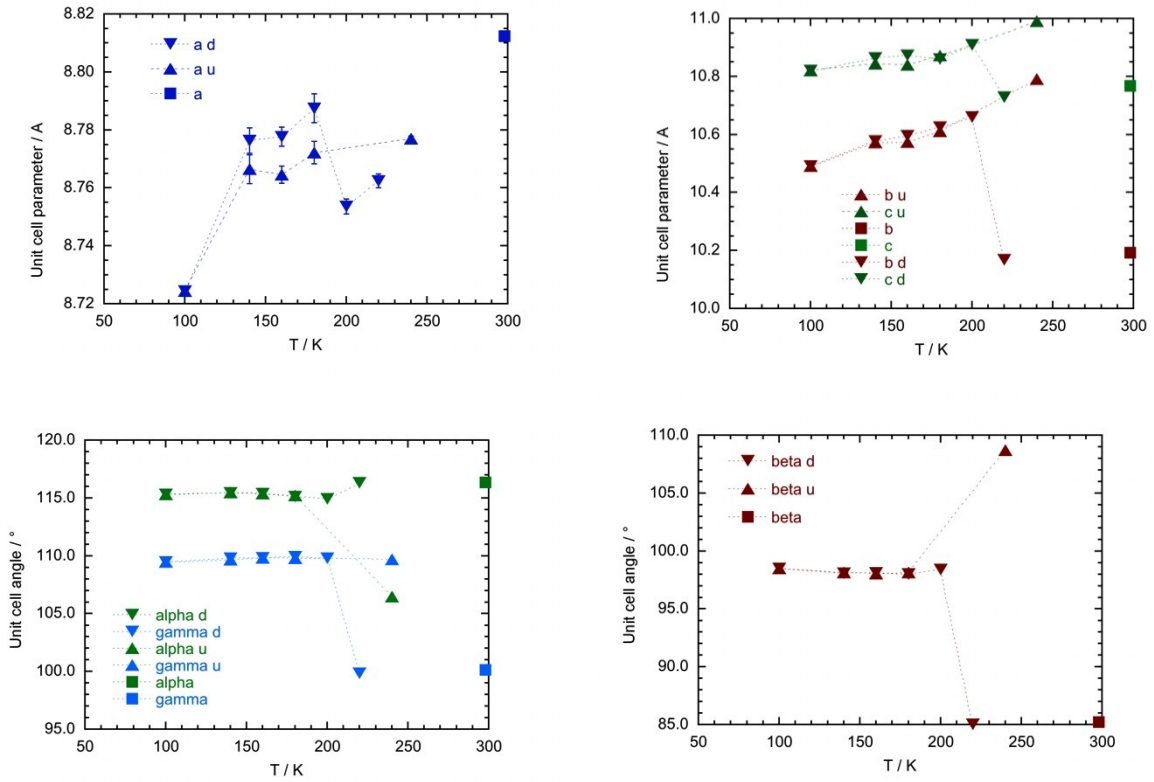

Fig. S7 : Relative unit-cell parameters of the triclinic polymorph of Fe[HB(3,5-$(Me)_2Pz)_3$] plotted as a function of temperature between 298 and 100 K : (②) and (①) markers for the cooling and heating mode.

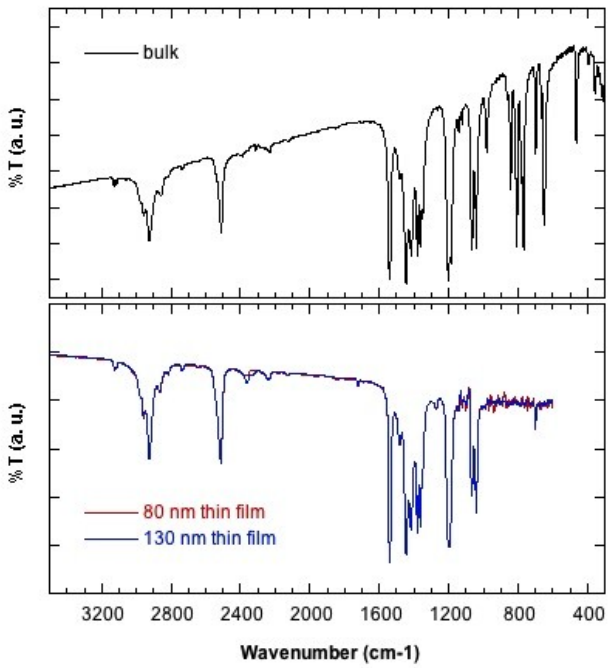

Fig. S8: RT IR spectra of Fe[HB(3,5-$(Me)_2Pz)_3]_2$ in form of bulk (dispersion in a KBr pellet) and 80 nm- or 130 nm (**1**)-thin layers (deposition on silicon wafers).

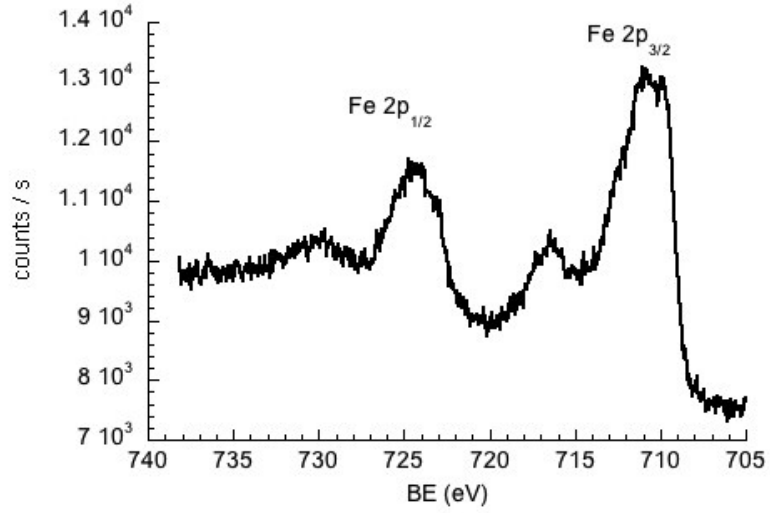

(a)

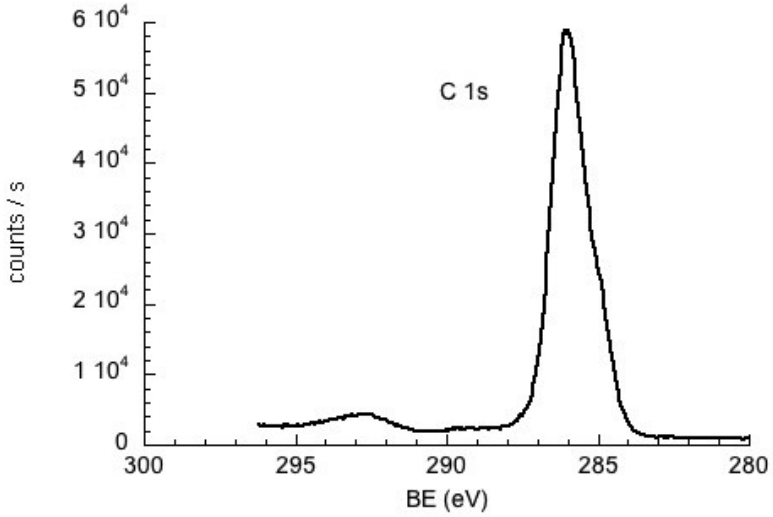

(b)

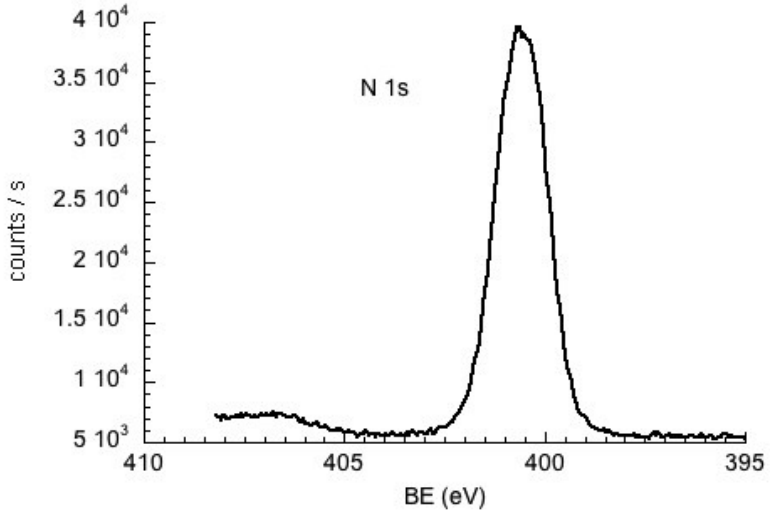

(c)

Fig. S9 : X-ray photoelectron spectra (Al-Kα) of the Fe(2p) (a), C(1s) (b) and N(1s) (c) core levels recorded with the 130 nm-thick layer (noted **1**) deposited on a silicon wafer.

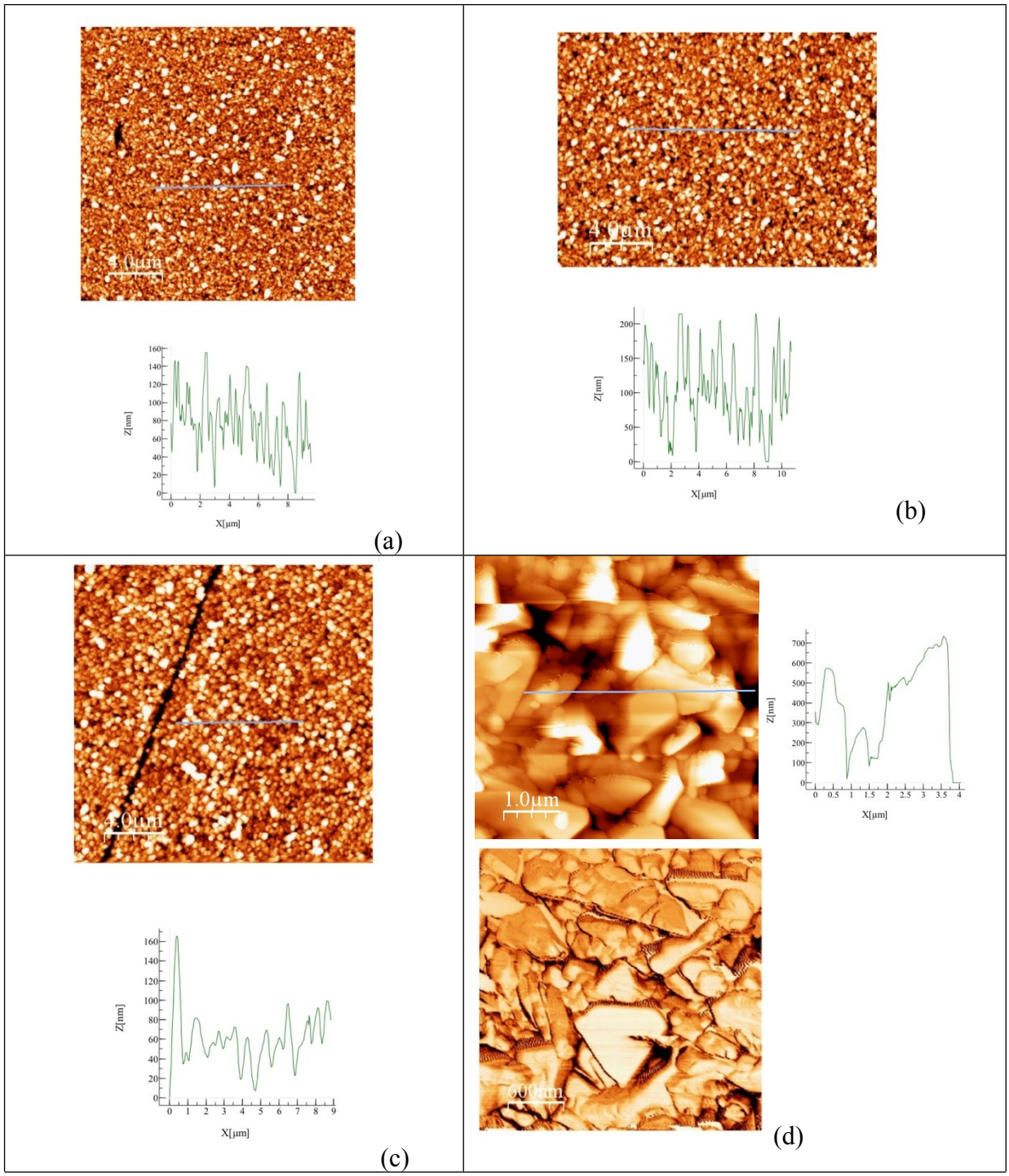

Fig. S10: AFM images of layers prepared with a thickness equal to : (a) 130 nm (as-sublimed, noted **1**) ; (b) 130 nm (after annealing, **1**); (c), 840 nm (after annealing); (d) 8020 nm (as sublimated, noted **2**).

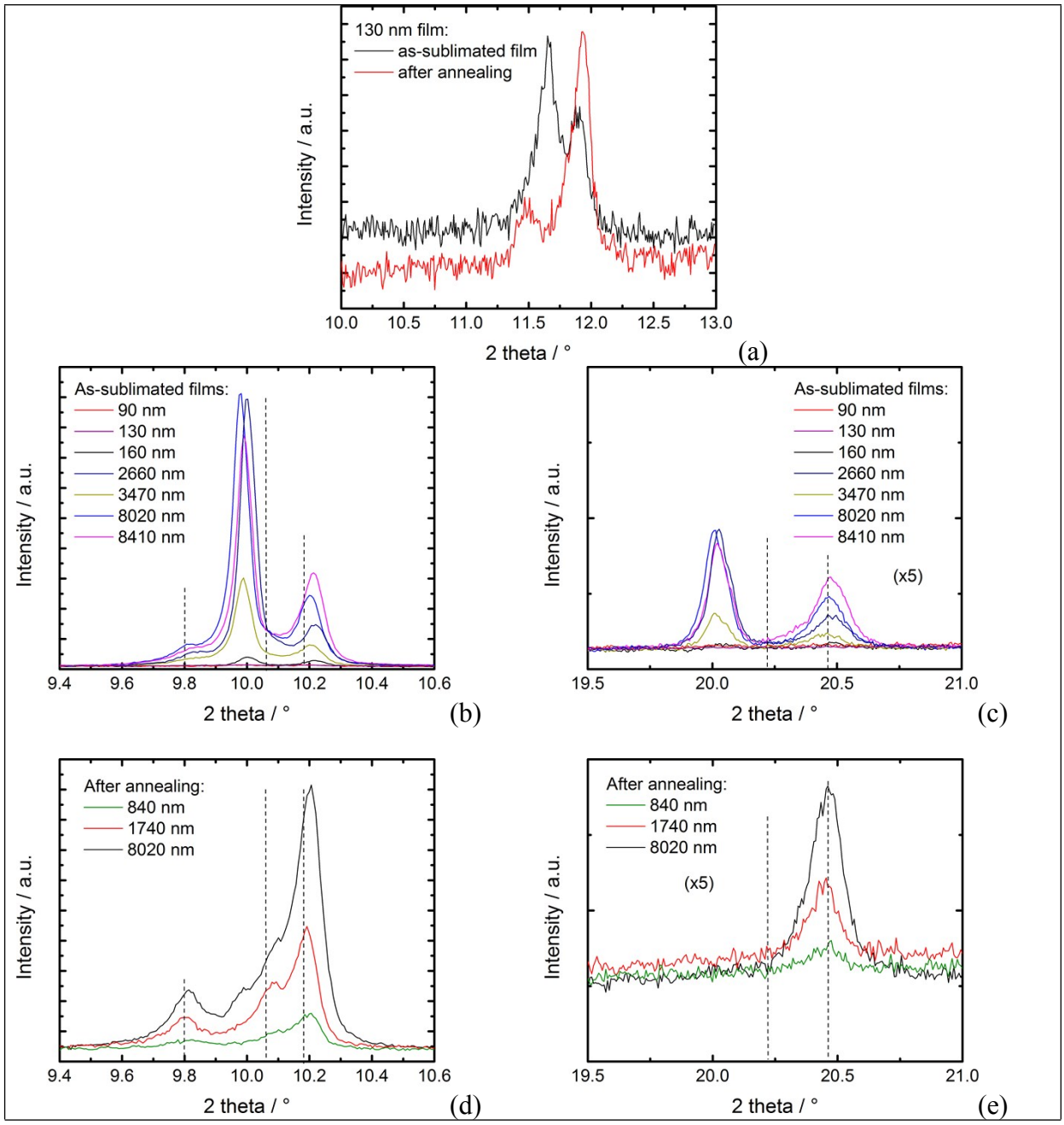

Fig. S11 : X-ray diffraction patterns of as-sublimed (a-c) and annealed (d,e) layers of $Fe[HB(3,5\text{-}(Me)_2Pz)_3]_2$ deposited on quartz. The 2θ angles refer to the (a) Co Kα (130 nm-thick layer) or (b-e) Cu Kα (other layer thicknesses) radiation and the angle positions of the *(010)*, *(01-1)*, *(100)*, *(02-2)* and *(200)* Bragg peaks of bulk phase are marked with dotted lines.

Sample	2θ angles (°) Cu Kα radiation				
As-sublimed film	9.2	9.8	9.96	-	10.2
Annealed film	9.2	9.8	-	(b)	10.2
Triclinic phase (a)	9.15	9.80	-	10.07	10.22
Bragg reflection	*(001)*	*(010)*	-	*(01-1)*	*(100)*

(a) at T = 298 K ; b, shoulder

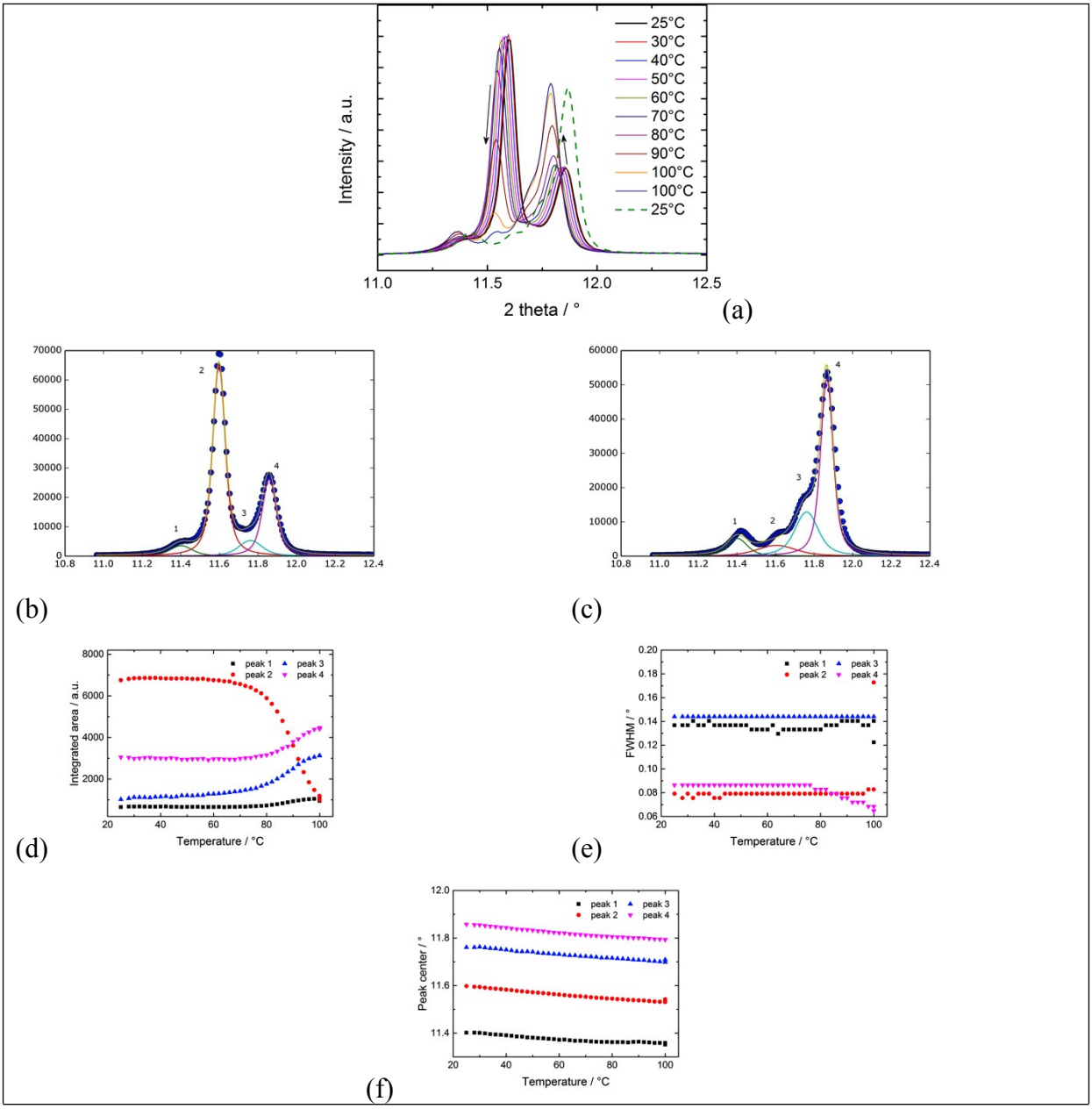

Fig. S12: (a) XRD patterns (Co Kα radiation) of the 8460 nm-thick layer recorded as a function of temperature between 298 and 373 K, then after the return to 298 K. Arrows indicate the evolution of the two main Bragg peaks upon the phase transformation ; (b, c) Experimental diffractograms at 298 K before (b) and after (c) annealing on which the pseudo-Voigt functions used for the fitting are superimposed ; (d-f) Evolution with the temperature of the area (d) ; width (e) and position (f) of Bragg peaks.

Sample	2θ angles (°) Co Kα radiation				
As-sublimed film	10.7 (c)	11.4	11.60	-	11.9
Annealed film	10.7 (c)	11.4	(d)	Ca. 11.7	11.9
Triclinic phase[a]	10.65	11.39	-	11.70	11.84
Bragg reflection	*(001)*	*(010)*	-	*(01-1)*	*(100)*

c, very weak, d, residual traces

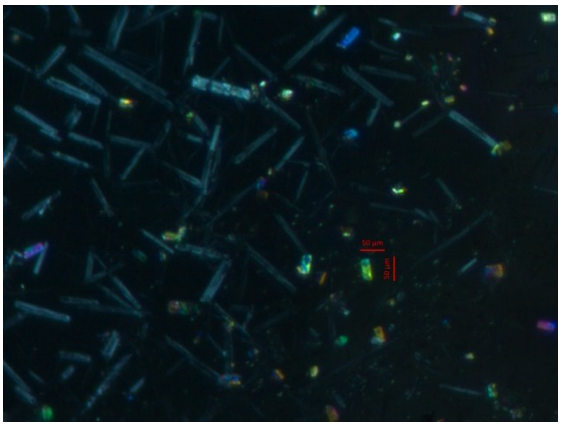

(a)

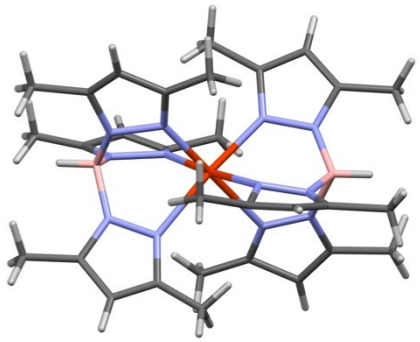

(b)

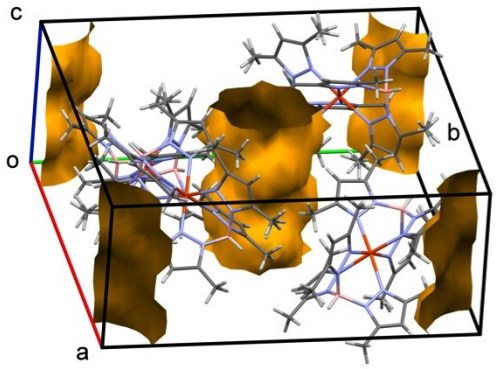

(c)

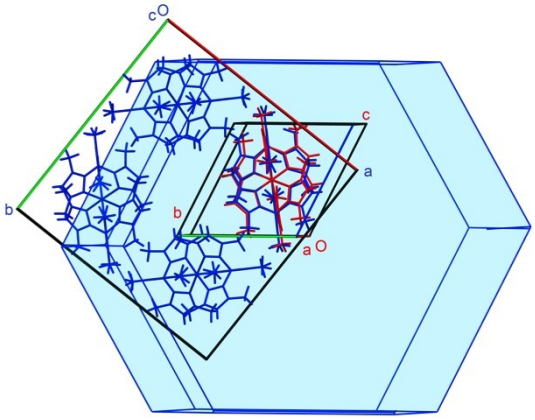

(d)

Fig. S13: (a) Photograph of the mixture of needle- and platelet-shaped microcrystals forming the as-sublimed 6810 nm-thick film; (b) View of the molecule and (c) the molecular packing characterizing the platelet (tetragonal polymorph, *P-4 2₁ m*) at 253 K. In yellow, is shown the void space occupied by solvent molecule in one unit-cell as determined by calculations conducted with the Mercury software (probe radius of 1.2 Å, grid spacing of 0.7 Å) ; (d) superposition of the diamondoid cages for *P-1* (red) and *P -4 2₁ m* (blue) along the [1 0 0] axis in the triclinic or [0 0 1] axis in the tetragonal polymorph. In light blue the representation of the preferential orientation of the platelets.

Comments on the tetragonal polymorph. The material forming the 6810 nm-thick film (Fig. S13) was removed by rinsing the surface with a nonsolvent (Et_2O). The photograph shows a mixture of needle- and platelet-like crystals. The platelet (dimensions: 30x20x10 μm^3) gave rather poor diffraction data which allowed the identification of a new polymorph of the complex shown in Fig. S13b, but did not permit a discussion of the structural details. It crystallizes in the quadratic system, space group *P-4 2₁ m* with a = b = 20.669(5) Å and c = 8.603(3) Å, V = 3675(2) $Å^3$ at T = 253K, containing four molecules per unit-cell.
Some residual electronic density was localized in the lattice. The hypothesis to consider was the inclusion of disordered solvent molecules in the channels of submicrometric size upon the wet treatment used for the removal of the polycrystalline powder. The modeling of unknown disordered molecules being non trivial, their contributions to the scattering were removed using the SQUEEZE procedure (Spek, A. L. *Acta Cryst*., 2015, **C71**, 9-18.) in PLATON (Spek, A. L. *Acta Cryst*., 2009, **D65**, 148-155.). SQUEEZE calculated a void

volume of approximately 434 Å^3 occupied by 87 electrons per unit cell, which points to the presence of some solvent molecule per formula unit. Fig. S13(c) shows the related positions of voids within the unit-cell. The given chemical formula and other crystal data do not take into account these solvent molecules.

One issue to address is the fact that the preferential orientation of the crystallites in the films was preserved upon the phase transformation due to the thermal annealing. In the as-sublimed films, the metastable phase is slightly different because of the absence of any solvent molecule. One reasonable hypothesis is to assume the same tetragonal structure with a simple expansion-contraction of the unit-cell parameters depending on the inclusion or extrusion of solvent molecules (Sanchez-Costa J. *et al J. Am. Chem. Soc*. 2014, **136**, 3869.) which is associated with the Bragg peak shift. In Fig. S13d, we show the orientation of the two unit-cells that would be consistent with the experimental observations: growth of the (100) Bragg peak upon heating and disappearance of the (*001*) peak (at 9.96°) of the metastable polymorph.

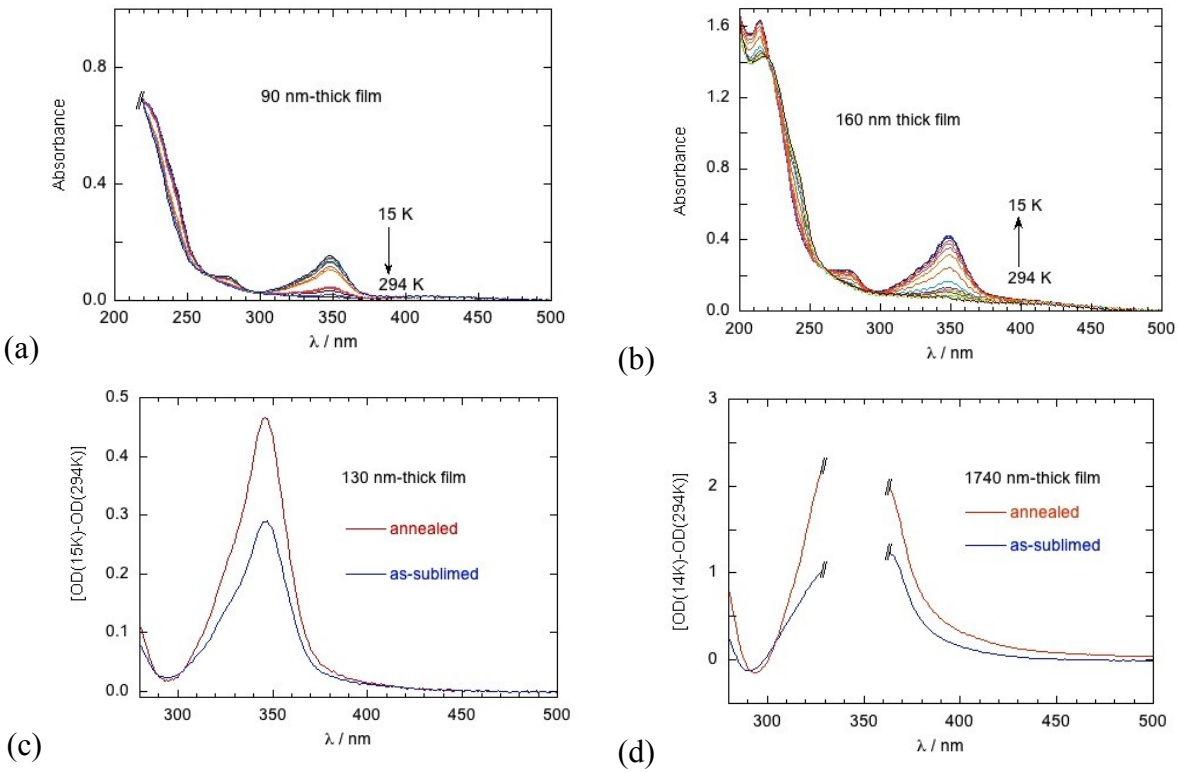

Fig. S14 : Variable temperature UV-vis spectra recorded with the as-sublimed films of Fe[HB(3,5-$(Me)_2Pz)_3]_2$ deposited on quartz. (a) 90 nm-thick film (b) 160 nm-thick film. Superimposition of the ΔOD spectra for the as-sublimed (blue) and annealed films (red) (with ΔOD = OD(15K)-OD(294K)): (c) 130 nm-thick film (noted **1**), (d) 1740 nm-thick film. The range marked with line breaks (d) corresponds to the signal saturation.

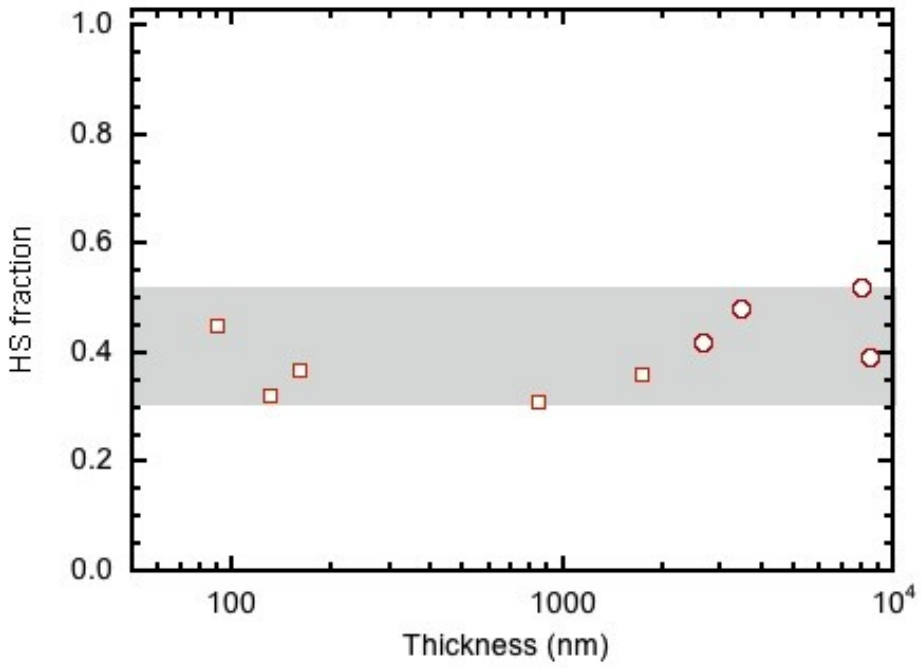

Fig. S15 : Plot of the fraction of HS residue in the as-sublimed samples as a function of the layer thickness. This population was estimated from the optical (□) and magnetic (○) measurements as described in the text or below. The grey area indicates the range of variation found for the HS residue.

Determination of the fraction of HS residue observed in the as-sublimed films. To quantify the change in the SCO population after the phase transformation, we exploited the linear dependence of ΔOD at 366 nm in the MLCT range *vs.* the thickness that was observed up to 1740 nm. If we consider, all things being equal, a complete SCO after annealing, as checked with optical measurement and supported by the magnetic data, we can write $\Delta OD_{annealed} / \Delta OD_{as\text{-}sublimed} = 1/(1- x^{HS}_{residue}) = k$ and determine the fraction of HS residue ($x^{HS}_{residue}$) in the as-sublimed layer.

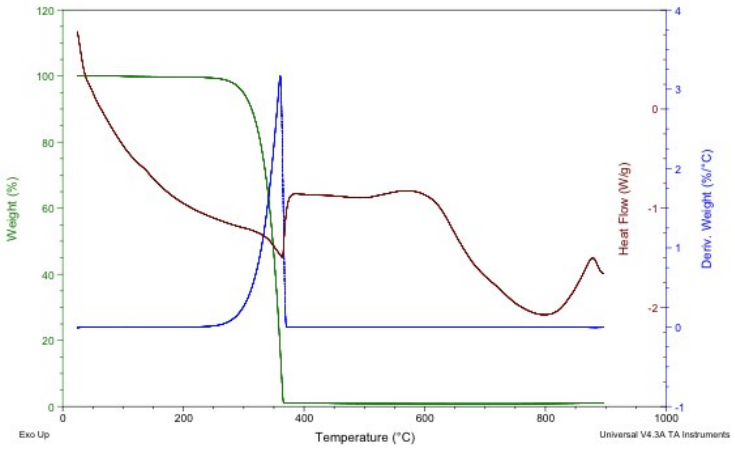

Fig. S16 : Thermogravimetry analysis of $Fe[HB(3,5\text{-}(Me)_2Pz)_3]_2$.